FULL LENGTH PAPER

COMPUTATION OF HEAT FLUX IN HYPERSONIC FLOW WITH A CARTESIAN MESH USING NEAR-WALL RESOLUTION

V. Ashok; George Joseph
Aerodynamics and Aerothermal Group
Vikram Sarabhai Space Centre, ISRO
Thiruvananthapuram-695 022,India
Email : v_ashok@vssc.gov.in

V. Adimurthy
Indian Institute of Space Science and Technology
Department of Space
Thiruvananthapuram-695 547 India

Abstract

A hybrid solution methodology is developed to solve laminar hypersonic flow with a Cartesian mesh approach. The hybrid grid consisting of a Cartesian mesh together with an unstructured prism layer near the wall to capture the large gradients close to the surface is used for the near wall viscous resolution. The prism layer is generated by extruding the panels formed by the intersection of the Cartesian grid and the body and is stitched with the outer Cartesian mesh away from the wall for solving axi-symmetric flows. For three dimensional flows, since the prism layer cells are not stitched to the outer Cartesian mesh, the inviscid solution is carried out first for background Cartesian mesh and later this solution is mapped to the extruded prism layer cells and laminar Navier-Stokes solution is carried out for the prism layer cells alone. The developed solver gives an unstructured prism layer solution near the wall and standard Cartesian mesh solution away from the wall. This hybrid solution methodology is validated against the experimentally measured heat flux data and could predict the heat flux with good accuracy. The present methodology thus enables the computation of a viscous solution using a Cartesian mesh based approach.

Nomenclature

a = speed of sound (m/s)
e = internal energy per unit mass (J/kg)
k = coefficient of thermal conductivity (W/m/K)
l = distance between centroids of cell i and cell j (m)
q = heat flux (W/sq.m)
u = velocity in X direction (m/s)
v = velocity in Y direction (m/s)
w = velocity in Z direction (m/s)
E = total energy per unit mass (J/kg)
H = total enthalpy per unit mass (J/kg)
M = Match number
P = pressure (Pa)
R = universal gas constant (8314.34 J/kg-mole K)
T = temperature (K)
U = vector of conserved variables
V = total velocity (m/s)
F_c = vector of convective flux
F_v = vector of viscous flux
p_c = cell center pressure of the wall cell (Pa)
S_x = projected area in x direction of each face (sq.m)
S_y = projected area in y direction of each face (sq.m)
S_z = projected area in z direction of each face (sq.m)
ΔU_i = cell centre gradient at cell i
ΔU_j = cell centre gradient at cell j
V = contravariant velocity at the face of the cell (m/s)
Λ_c = convective spectral radius (m/s)
σ = CFL number
$\vec{l_{ij}}$ = unit vector of line connecting cell centroids i and j
Ω = volume (m^3)
Δt = local time step of the cell (s)
τ_{xx} = normal stress in the X-plane and in X direction (N/m^2)
τ_{xy} = tangential stress in the X-plane and in Y direction (N/m^2)
τ_{xz} = tangential stress in the X-plane and in Z direction (N/m^2)

Paper Code : V65 N2/779-2013. Manuscript received on 27 Apr 2012. Reviewed, revised and accepted as a Full Length Contributed Paper on 26 Oct 2012

Pr = Prandtl number
Re = Reynolds number
μ = Coefficient of viscosity (kg/m-s)
γ = Specific heat ratio
ρ = Density (kg/ m^3)
n_x, n_y, n_z = Direction cosines of normal
α = Angle of attack (deg)

Subscripts

c = Convective
v = Viscous
$_c$ = Cell center
$_{x,y,z}$ = x, y, z direction
$_{wall}$ = Wall
0 = Stagnation
∞ = Free stream
inf = Free stream

Introduction

Cartesian mesh has an advantage in terms of automated grid generation for complex geometries, which makes it quite useful in aerospace industry. However, it has a serious limitation to handle the viscous boundary layer near the wall. There have been considerable efforts in the last decade to overcome this limitation through different approaches like hybrid meshes, immersed boundary methods, meshless methods and even pure Cartesian mesh [1-12]. The literature shows Cartesian/prism method in which an adaptive Cartesian grid and a fixed prism grid are combined to tackle viscous flows. A nested multi-grid viscous flow solver for body fitted adaptive quadrilateral grids around solid bodies through surface extrusion, which are then overlapped with an adaptive Cartesian grid is also reported [2]. Multi-solver approach is also reported which has curvilinear grids near the solid boundaries and Cartesian grid away from the body to fill majority of the boundary domain and the interface being handled by an edge based grid free solver [3]. Hybrid Cartesian-body fitted grid is another method wherein a near wall boundary is automatically searched for a given geometry, which merges with a Cartesian background grid without any overlap [4]. A good amount of work is reported on immersed boundary technique [5-10] in which locally refined Cartesian mesh is used to solve three dimensional Navier-Stokes equations. The viscous flow solution with Cartesian mesh stitched to the wall and termed as Cartesian like grids is also reported to give good solution with Navier-Stokes equation for aerofoils in certain range of Reynolds numbers [11]. Solution of two dimensional high Reynolds number turbulent flow is reported with even pure Cartesian mesh solver [12]. In this method small cut cells are merged with the neighboring cells and local mesh refinement is adapted to have a fine resolution near the wall. However this approach leads to a very large number of cells for three dimensional flows. The present paper describes a hybrid solution methodology to solve laminar hypersonic flow with a Cartesian mesh based approach. All the methods mentioned above have not been applied to hypersonic flows so as to obtain heat flux. The present solution methodology differs from the previous approaches in the literature in the sense that in this approach, the extrusion of background Cartesian mesh panels obtained after the Cartesian mesh generation is done to capture the large gradients near the wall and this prism layer is in turn stitched with the outer Cartesian mesh away from the wall and applied to obtain heat flux on the wall.

Problem Definition

To validate, the hybrid solver, a standard AGARD HB-2 model, which is a sphere-cone-cylinder-flare geometry, with a core diameter of 100mm as shown in Fig.1 is chosen and for which hypersonic wind tunnel data [18] are available in the open literature. The experiments are conducted in JAXA 1.27 m blow-down cold type hypersonic wind tunnel and one of the objectives of the tests is for generating good quality experimental results for HB-2 geometry, which would serve as benchmark for hypersonic computational fluid dynamics codes. The free stream conditions for which the numerical simulations are carried out is shown in Table-1.

Gridding Strategy

The initial Cartesian mesh is generated with a 100 x 100 x 1 basic mesh as shown in Fig.2. The hybrid mesh

Table-1 : Free Stream Conditions

P_0 (Mpa)	T_0 (K)	M_∞	ρ_∞ (kg/m^3)	T_∞ (K)	P_∞ (Pa)	U_∞ (m/sec)	Re ($x10^5$) based on core dia	α (deg)	T_{wall} (K)	μ (kg/m-s)
2.512	1025.8	9.59	0.00469	55.3	74.5	1429.6	1.85	0	300	$3.62x10^{-6}$

with prism layer upto 40mm, 30mm and also up to 20mm are generated and subsequently stitched with outer Cartesian mesh. The 40mm prism layer has 45 cells with a stretching factor of 1.14 yielding a first cell height of 15 microns and 30mm prism layer has 55 cells with a stretching factor of 1.1 giving first cell height of 16 microns. Computations are carried out with two 20mm prism layer mesh having 55 cells with a stretching factor 1.1 and 1.12 yielding a first cell height of 10 microns and 5 microns respectively. This exercise is done to see the effect of prism layer mesh on the solution, especially the heat flux on the wall.

Initially a Cartesian mesh is generated for the body using an existing Cartesian mesh code. The Cartesian mesh that is generated for arbitrary three-dimensional body gives rise to surface panels of 3 sides to 6 sides. To generate the prism layer for each panel, the normal at each nodal point of the body panel is obtained by average of all the normals that share the particular node. This extrusion follows an algebraic stretching function for which the user specifies the stretching factor. Normally this stretching factor used is of the range from 1.05 to 1.2. Fig.3 shows the Cartesian mesh for the nose of the present geometry and the hybrid mesh for select panels.

The details of the hybrid Cartesian mesh generation are given below.

- Start with the Cartesian mesh having information on the intersection point of mesh with the body. The surface of the body is essentially the panels formed by intersection of Cartesian mesh with the body. For 3D geometry, the surface panels have 3 to 6 sides whereas for a 2D geometry surface panels have 4 sides with one grid in the third direction as in the present problem.
- The normal of each panel corresponds to the normal of the largest triangle of the panel. Find out the average normal at each node which is essentially the average of the normal of the panels sharing the node.
- Since the Cartesian mesh would sometimes give rise to very small panels while cutting a body, the small panels whose area is less than $1/10^{th}$ of the neighbouring panel is merged with the large panel.
- Generation of the hybrid prism layer by extrusion of the surface panels is upto a height that is user specified. Normally extrusion is based on the average normal of a node. However this can also be user defined way of projection for ease of stitching with the outer Cartesian mesh.
- Stitch the prism layer with the outer Cartesian mesh by joining the prism layer to the nearby outer Cartesian mesh node.
- Split the last hybrid layer if it is too large as compared to neighbouring prism layer.

Figures 4 to 7 show the various steps of the hybrid prism layer generation and finally stitched with the outer Cartesian mesh. Fig.7 shows the final hybrid Cartesian mesh and the magnified region of the nose and flare portion. From the figure it can be seen that there are five types of cells possible after the stitching of hybrid prism layer with the outer Cartesian mesh. The first type of cell is the hybrid prism layer whose neighbours are also prism layer cells. The second type of cell is an edge cell which is between the prism layer cell and the Cartesian mesh which can have more than one Cartesian cell as its neighbour. The third type of cell is the outer hybrid prism layer hugging the Cartesian mesh which can have more than one Cartesian mesh as its neighbor. The fourth type of cell is the Cartesian cell where all the neighbours are not pure Cartesian cells and finally the fifth type of cell is the one whose all neighbours are Cartesian cells.

Boundary Conditions

The wall boundary conditions are the no-slip boundary conditions for velocities and cold wall conditions for energy equation. Since the flow is supersonic, supersonic outflow boundary condition is applied at flow leaving boundary. For axi-symmetric problems appropriate symmetry boundary conditions are applied.

Solution Methodology

The governing Navier-Stokes equations using the standard notation is as follows

$$\frac{\partial}{\partial t}\int_{\Omega} U\, d\,\Omega + \oint \left(F_c - F_v\right) d\,S = 0 \qquad (1)$$

Where U is vector of conserved variables and F_c and F_v are vector of convective and viscous fluxes respectively as given below

$$U = \begin{bmatrix} \rho \\ \rho u \\ \rho v \\ \rho w \\ \rho E \end{bmatrix} \quad F_c = \begin{bmatrix} \rho V \\ \rho u V + n_x p \\ \rho v V + n_y p \\ \rho w V + n_z p \\ \rho H V \end{bmatrix}$$

$$F_v = \begin{bmatrix} 0 \\ n_x \tau_{xx} + n_y \tau_{xy} + n_z \tau_{xz} \\ n_x \tau_{yx} + n_y \tau_{yy} + n_z \tau_{yz} \\ n_x \tau_{zx} + n_y \tau_{zy} + n_z \tau_{zz} \\ n_x \theta_x + n_y \theta_y + n_z \theta_z \end{bmatrix} \tag{2}$$

$$V = u n_x + v n_y + w n_z \tag{3}$$

$$H = e + \frac{u^2 + u^2 + w^2}{2} \frac{p}{\rho} \tag{4}$$

$$\begin{aligned} \theta_x &= u \tau_{xx} + v \tau_{xy} + w \tau_{xz} + k \frac{\partial T}{\partial x} \\ \theta_y &= u \tau_{yx} + v \tau_{yy} + w \tau_{yz} + k \frac{\partial T}{\partial y} \\ \theta_z &= u \tau_{zx} + v \tau_{zy} + w \tau_{zz} + k \frac{\partial T}{\partial z} \end{aligned} \tag{5}$$

$$\tau_{xx} = 2\mu \left(\frac{\partial u}{\partial x} - \frac{1}{3} (\partial u/\partial x + \partial v/\partial y + \partial w/\partial z) \right) \tag{6}$$

$$\tau_{yy} = 2\mu \left(\frac{\partial v}{\partial y} - \frac{1}{3} (\partial u/\partial x + \partial v/\partial y + \partial w/\partial z) \right) \tag{7}$$

$$\tau_{zz} = 2\mu \left(\frac{\partial w}{\partial z} - \frac{1}{3} (\partial u/\partial x + \partial v/\partial y + \partial w/\partial z) \right) \tag{8}$$

$$\tau_{xy} = \mu \left(\frac{\partial u}{\partial y} + \frac{\partial v}{\partial x} \right) \tag{9}$$

$$\tau_{xz} = \mu \left(\frac{\partial u}{\partial z} + \frac{\partial w}{\partial x} \right) \tag{10}$$

$$\tau_{yz} = \mu \left(\frac{\partial v}{\partial z} + \frac{\partial w}{\partial y} \right) \tag{11}$$

Where V is the contravariant velocity at the face of the cell, n_x , n_y , n_z are the direction cosines of the outward normal to a face of the cell, e is the internal energy, H is the enthalpy, and u,v,w are the Cartesian velocity components in the x,y and z directions.

The coefficient of molecular viscosity μ is obtained from Sutherland's law wherein the coefficient of viscosity is a function of temperature and coefficient of thermal conductivity k is also obtained as a function of temperature [13]. Perfect gas law has been used and is valid throughout the flow field.

The wall boundary conditions are applied by invoking the characteristic based boundary conditions [14]

$$p_{wall} = p_c - a (\rho u n_x + \rho v n_y + \rho w n_z) \tag{12}$$

The heat flux on the wall is obtained from the numerical solution based on the coefficient of thermal conductivity of the cell adjacent to wall and the wall temperature gradient at the wall and is expressed as given below

$$q_{wall} = -k \left[\frac{\partial T}{\partial n} \right]_{wall} \tag{13}$$

To achieve second order accuracy, the linear reconstruction of the primitive variables is done to get the interface values and inviscid fluxes are obtained using the AUSM [15] solution. The Venkatakrishnan limiter [16] is used to limit the gradients during reconstruction. The cell centre gradients are evaluated by the standard Green-Gauss procedure and the interface gradients, which are used for estimation of viscous fluxes, are estimated using the following expression [17]

$$\nabla U_{ij} = \bar{\nabla} U_{ij} - \left(\bar{\nabla} U_{ij} \cdot \vec{t_{ij}} - \left(\frac{\partial U}{\partial t} \right)_{ij} \right) \vec{t_{ij}} \tag{14}$$

where

$$\bar{\nabla} U_{ij} = \frac{1}{2} \left(\nabla U_i + \nabla U_j \right) \tag{15}$$

and $\vec{t_{ij}}$ = Unit vector of line connecting Cell centroids i and j

∇U_i and ∇U_j = Cell centre gradient at Cell i and Cell j respectively

l = Distance between centroids of Cell i and Cell j

The scheme is fully explicit and time marching is done with local time stepping which is calculated as below

$$\Delta t_{cell} = \sigma \frac{\Omega_{cell}}{(\Lambda^x_c + \Lambda^y_c + \Lambda^z_c)_{cell} + (\Lambda^x_v + \Lambda^y_v + \Lambda^z_v)_{cell}} \quad (16)$$

where σ is the CFL number which is less than 0.5 for a stable solution since the scheme is fully explicit and Λ^x_c, Λ^y_c, Λ^z_c are the convection spectral radii which are given as

$$\Lambda^x_c = (|u| + a)\Delta S_x, \Lambda^y_c = (|v| + a)\Delta S_y, \text{ and}$$
$$\Lambda^z_c = (|w| + a)\Delta S_z \quad (17)$$

The viscous spectral radii for the x direction is expressed as

$$\Lambda^x_v = \max\left(\frac{4}{3\rho}, \frac{\gamma}{\rho}\right)\left(\frac{\mu_{laminar}}{Pr_{laminar}}\right)\left(\frac{(\Delta S_x)^2}{\Omega_{cell}}\right) \quad (18)$$

Ω_{cell} is the volume of the cell and ΔS_x, ΔS_y, ΔS_z are the projections of the control volume on y-z, x-z and x-y plane. These are given by the formulae

$$\Delta S_x = \frac{1}{2}\sum_{J=1}^{N_F} |S_x|_J$$
$$\Delta S_y = \frac{1}{2}\sum_{J=1}^{N_F} |S_y|_J \quad (19)$$
$$\Delta S_z = \frac{1}{2}\sum_{J=1}^{N_F} |S_z|_J$$

Where S_x, S_y and S_z, and are the projected area in the x, y and z direction of each face and N_F is the number of faces of the cell. The hybrid solver program is written in C language with an appropriate data structure for panel and hybrid cell. Each panel corresponds to the partial cell of the Cartesian mesh. The panel data structure contains the information on normal, number of sides of panel, area and node numbers and their coordinates and information about its neighbouring panels. It also has the pointer to the hybrid cell array above the panel. Similarly for each hybrid cell, the data structure has all the information about its faces, neighbour of each face, cell center coordinates, volume and conserved variable vector. The code is written keeping in mind a general three dimensional case although the sample case present in this paper is an axi-symmetric solution.

Results and Discussion

Figure 8 shows the wall heat flux along the length of the body for various iterations for 20mm prism layer with 55 cells in which the first cell height is 5 microns. The iteration convergence is clearly seen after 20000 iterations and for this case all the residues had reduced by more than 3 orders of magnitude.

Figures 9 and 10 show the Mach number profile at two typical stations with Mach palette to see whether the prism layer height has any influence on the profiles and especially in the region of transition from the unstructured prism layer to the Cartesian mesh. It is seen that the Mach number profiles at the two typical stations is almost same and shows that the solutions are grid independent. As expected the boundary layer starts becoming thicker as the axial distance increases. The Mach line contours with values marked and showing the expansion waves and oblique shock is also presented in Fig.11.

Figures 12 to 14 show the pressure, temperature and Mach number along the body obtained from the pure Cartesian mesh Euler solution which would correspond to the boundary layer edge conditions. The pressure is maximum at the stagnation point followed by continuous expansion till the cylinder after which the pressure is constant and then a further rise is observed at the start of the flare due to the oblique shock at the cylinder flare junction. The Mach number along the body is shown in Fig.13 which shows continuous increase till the flare after which the Mach number falls due to the oblique shock and the temperature distribution along the axial distance is shown in Fig.14 which corresponds to the behaviour of the pressure and Mach number plots. Fig.15 shows the static temperature, total temperature and total velocity profile at a typical station 0.374m plotted along the vertical height from the wall. The temperature in the boundary layer initially increases due to the viscous dissipation and then gradually achieves the free stream temperature. The total temperature achieves the maximum value at around 1cm from the wall and is constant beyond this height as expected. The total velocity profile is also on the expected line. Fig.16 shows the plot of static density profile at the

station 0.374m from nose. The density at the wall is minimum in the boundary layer portion were static temperature is highest and gradually increases as the distance from the wall increases reaching a maximum value at the shock location and subsequently reducing to free stream value. Fig.17 shows the plot of stagnation density along the vertical height from the wall at the location 0.374m with small increase in the boundary layer portion and then increasing sharply beyond this and finally reaching the stagnation density value at a distance of about 11cm from the wall.

Figure 18 shows the comparison of computed heat flux for the HB-2 geometry with that of the experimental results [18]. The heat flux is maximum at the stagnation point and decreases sharply as the flow expands over the conical region and then remains nearly constant in the cylindrical region with slight increase in the flare region due to compression. The plot shows that the results are clearly grid independent and also good match with the experimental data is seen from the computation. The enlarged view of the heat flux comparison is given in Fig.19 to show the prediction of the heat flux in expansion as well as compression regions of the geometry. The present methodology demonstrated for an axi- symmetric geometry to obtain the near wall resolution of a laminar hypersonic flow from a Cartesian mesh based approach can be considered as the first step before extending to three dimensional geometries.

Heat Flux Estimation for a Typical Bulbous Heat Shield Configuration

The present hybrid solution methodology is also applied to a typical bulbous heat shield geometry for which the shock tunnel experimental results are available at hypersonic mach numbers [19]. The geometric details are given in Table-2 and Fig.20. The free stream conditions are given in Table-3.

The computations are carried out with hybrid mesh consisting of prism layer of 20mm stitched to the outer Cartesian mesh. The computations are done for laminar flow conditions as in the tunnel. The first grid point is of the order of 11 microns with about 45 number of prism layer cells.

Figure 21 shows the heat flux along the length of the model which gives a reasonable match with the shock tunnel measurements. The maximum heat flux of about 119 W/sq.cm is computed at stagnation point against the experimental measurement of 114 W/sq.cm.

This is followed by a steep fall due to the expansion and nearly constant in the cone portion followed by a drop in the heat flux after the cone due to the expansion at the cone cylinder junction and after little downstream of the cylindrical region constant heat flux is observed followed by further small drop in the boat tail region. After the boat tail a slight increase in heat flux is noticed due to compression and remains constant after the pressure recovery in the cylinder.

Hybrid Solution for Three Dimensional Flows

After reasonable validation of the hybrid solution methodology to axi-symmetric flows, the next logical step is to extend it to three dimensional flows. As a first step to extend this method to three dimensional flows, initially an Euler solution is obtained over the body with the Cartesian mesh. In the subsequent step, the prism layers are extruded from the background Cartesian mesh panels up to a certain height and the Cartesian mesh Euler solution obtained in the first step is mapped to this prism layer. Subsequently, the laminar viscous solution is carried out for this prism layer of cells alone and the outer boundary condition for the prism layer cells will be the Cartesian mesh solution. It is to be noted that, in this case, the interaction of the viscous layer would not be considered with the outer inviscid solution and hence will be similar to the boundary

Table-2 : Geometry Details of a Typical Bulbous Heat Shield

D1 (mm)	Rn/D1	θc (°)	L1/D1	θb (°)	D1/D2	L2/D2	L (mm)
50	0.2188	20	1.4062	15	1.1429	1.5	195

Table-3 : Flow Conditions of the Shock Tunnel Experiment (Ref.19)

M_∞	P_∞	ρ_∞	T_0	T_{wall}	R_e based on 50mm dia	α (Angle of Attack)
5.75	1320 Pa	0.019 kg/m^3	1829 K	300 K	1.143 x 10^5	0

Table-4 : Free Stream Conditions for Flow Over HB-2 Geometry at Angle of Attack (Ref.18)

P_0 (MPa)	T_0 (K)	M_∞	P_∞ (Pa)	ρ_∞ (kg/m^3)	T_∞ (K)	Re (1 x 10^5) based on core dia	α (deg)	T_{wall} (K)	U_∞ (m/s)
4.021	1040.7	9.65	114.7	0.00719	55.6	2.85	15	300	1441.9

layer type of solution. However if the prism layer cells are stitched to the outer Cartesian mesh then this interaction would automatically be taken into account as in the hybrid solution methodology described for axi-symmetric flows in the previous section. The stitching of this prism layer of cells in a three dimensional case with the outer Cartesian mesh is a very involved task and is planned to be taken up in the next phase of this work. However in many cases, if the prism layer is extended sufficiently to a distance beyond the interaction region, this in itself would give good solution. In order to demonstrate this methodology, a three dimensional flow case for the HB-2 geometry described in Fig.1 is chosen for which the free stream conditions are given in Table-4.

In the first step, an Euler solution is obtained for the pure Cartesian mesh for the free stream conditions at angle of attack 15 degrees. In the next step, unstructured prism layer is generated from the Cartesian mesh panels on the body for a distance of 40mm in the normal direction from the wall with 45 numbers of prism layer cells and the Euler solution is mapped to the unstructured prism layer. Subsequently, laminar Navier-Stokes equation is carried out for the prism layer alone with Euler solution boundary condition imposed for the outer layer of prism cells. Fig.22 shows the ratio of the heat flux to the stagnation point heat flux plotted along the windward side of the sphere cone cylinder flare geometry. The figure shows that the computed non-dimensional heat flux distribution along the body with the hybrid solution methodology shows a reasonable match with the experimentally measured data obtained from reference 18. The stagnation point is slightly downstream of the nose cap starting point due to angle of attack effect. The stagnation point heat flux obtained from the present computation is 20.3 W/sq.cm against the experimentally obtained value of 18.23 W/sq.cm. Also at the nose cap starting point, the computation shows a higher non dimensional heat flux of 0.98 as compared to the experimentally measured value of 0.95.

Conclusions

A Cartesian mesh based hybrid solution methodology to resolve the near-wall viscous region in a laminar hypersonic flow is demonstrated for a typical sphere-cone-cylinder-flare geometry and bulbous heat shield geometry. The Cartesian mesh based approach consists of building prism layer from the basic Cartesian mesh intersecting the body and subsequently stitching the extruded prism layer with the outer Cartesian mesh and this method is demonstrated for axi-symmetric flows. For three dimensional geometries, as a first step, Euler solution is obtained and this is mapped to the hybrid prism layer and subsequent laminar Navier-Stokes solution for the prism layer alone is carried out. The stitching of the prism layer mesh with the outer Cartesian mesh for three dimensional geometries is the future work identified. The hybrid solution methodology is a combination of unstructured mesh solution for the near wall prism layer and Cartesian mesh solution away from the wall. Heat flux computed for a typical cone cylinder flare geometry and bulbous heat shield type configuration shows good comparison with the reported experimental results.

Acknowledgements

Authors acknowledge Prof. N.Balakrishnan, Department of Aerospace Engineering, Indian Institute of Science, Bangalore, India for useful technical discussions and Dr. S.L.N. Desikan, Experimental Aerodynamics Division, Vikram Sarabhai Space Centre, Thiruvananthapuram, India for active support in preparing this manuscript.

References

1. Karman, S.L., "SPLITFLOW, 3D Unstructured Cartesian/Prismatic Grid CFD Code for Complete Geometries", AIAA Paper, 1995-0343.

2. Wang, Z.J., "A Fast Nested Multi-grid Viscous Flow Solver for Adaptive Cartesian/Quad Grids", International Journal for Numerical Methods in Fluids, 33, 2000, pp.657-680.

3. Katz, A., Jameson, A. and Wissink, A. M., "A Multi-Solver Scheme for Viscous Flows Using Adaptive Cartesian Grids and Meshless Grid Communication", AIAA Paper, 2009-768.

4. Chen, X. and Zha, G. C., "A Hybrid Cartesian-Body Fitted Grid Approach for Simulation of Flows in Complex Geometries", AIAA Paper, 2009-3880.

5. Tullio, M. D., Palma, P. D., Iaccarino, G., Pascazio, G. and Napolitano, M., "An Immersed Boundary Method for Compressible Flows Using Local Grid Refinement", Journal of Computational Physics, 225, 2007, pp. 2098-2117.

6. Mittal, R. and Iaccarino, G., "Immersed Boundary Methods", Annual Review of Fluid Mechanics, 37, 2005, 239-61.

7. Gilmanov, A. and Sotiropoulos, F., "A Hybrid Cartesian /Immersed Boundary Method for Simulating Flows with 3D, Geometrically Complex Moving Bodies", Journal of Computational Physics, 2005.

8. Kalitzin, G. and Iaccarino, G., "Towards Immersed Boundary Simulation of High Reynold Number Flows", Centre for Turbulence Research, Annual Briefs, 2003.

9. Kang, S., "An Improved Immersed Boundary Method for Computation of Turbulent Flows with Heat Transfer", Ph.D Dissertation, 2008, Stanford University.

10. Cho,Y., Chopra, J. and Morris, P. J., "Immersed Boundary Method for Compressible High Reynolds Number Viscous Flow Around Moving Bodies", AIAA Paper, 2007-125.

11. Mondal, P., Munikrishna, N. and Balakrishnan, N., "Cartesian Like Grids Using a Novel Grid Stitching Algorithm for Viscous Flow Computations", Journal of Aircraft, 44 (5), 2007, pp.1598-1609.

12. Kidron,Y., Yossef, Y. M. and Levy,Y., "Robust Cartesian Grid Flow Solver for High Reynolds Number Turbulent Flow Simulations", AIAA Journal, Vol.48, No.6, 2010, pp.1130-1140.

13. Kadoya, K., Matsunaga, N., Nagashima, A., "Viscosity and Thermal Conductivity of Dry Air in the Gaseous Phase", J. Phys. Chem., Ref. Data, Vol.14, No.4, 1985, pp.947-970.

14. Toro, E. F., "Riemann, Solvers and Numerical Methods for Fluid Mechanics: A Practical Introduction", Springer Edition, 2009.

15. Liou, M. S. and Stefen,C. J.Jr., "A New Flux Splitting Scheme", Journal of Computational Physics, 107, 1993, pp.23-39.

16. Venkatakrishnan,V., "Convergence to Steady State Solutions of the Euler Equations on Unstructured Grids with Limiters", Journal of Computational Physics, 118, 1995, pp.120-130.

17. Weiss, J.M. Maruszweski, J.P. and Smith,W. A., "Implicit Solution of Preconditioned Navier-Stokes Equations Using Algebraic Multigrid", AIAA Journal, 37, 1999, pp.29-36.

18. Kuchi-Ishi, S., Watanabe, S., Nakakita, K. and Koyama, T., "Comparative Force/Heat-flux Measurements Between JAXA Hypersonic Test Facilities Using Standard Model HB-2 (Part-1: 1.27m Hypersonic Wind Tunnel Results)", JAXA-RR-04-035E-March, 2005.

19. Srinivasa, P., "Experimental Investigation of Hypersonic Flow Over a Bulbous Heat Shield at Mach Number 6", Ph.d Thesis, Indian Institute of Science, Bangalore, 1991.

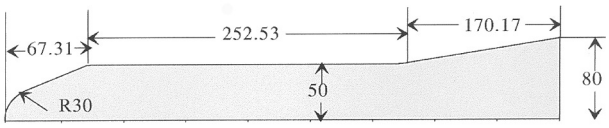

Fig.1 HB-2 Geometry [Ref.18] - (All dimensions in mm)

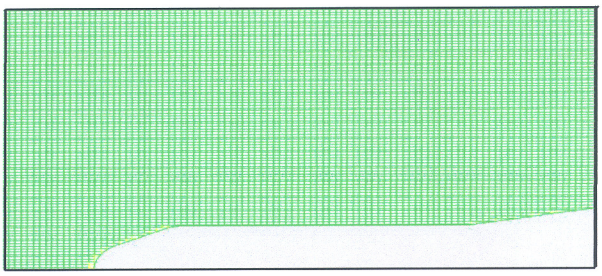

Fig.2 Based Cartesian Mesh for HB-2 Geometry

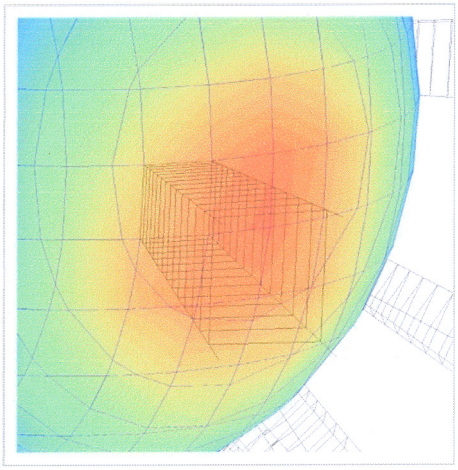

Fig.3 Panels Obtained from Cartesian Mesh Intersecting Three Dimensional Body (Nose Cone Portion) and Prism Layer for a Select Panel

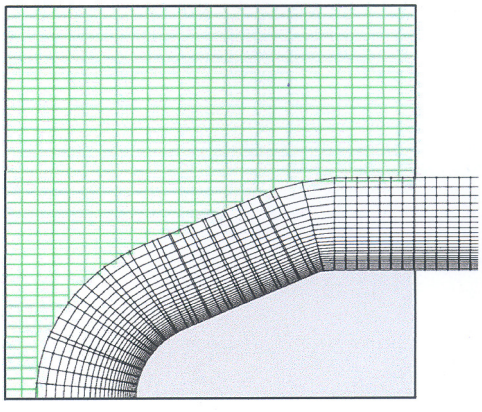

Fig.4 Prism Layer at Sphere Cone Region Without Merging of Small Panels

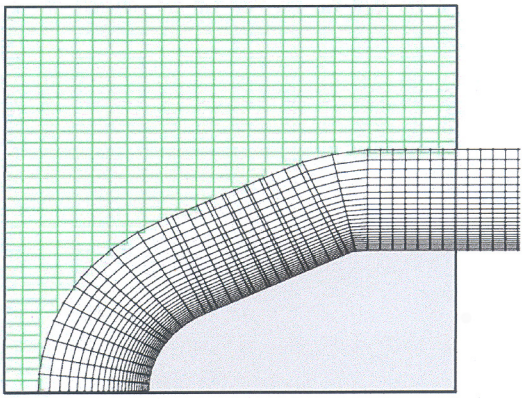

Fig.5 Prism Layer at Sphere Cone Region with Merging of Small Panels

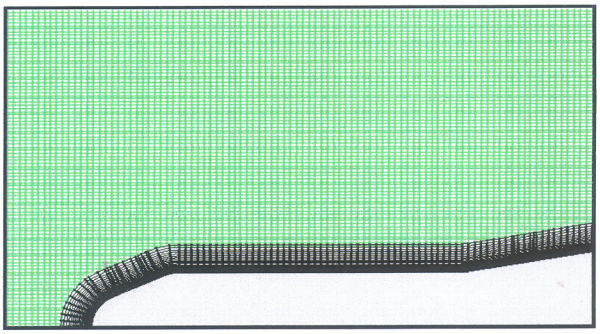

Fig.6 Prism Layer Mesh for the Full Geometry

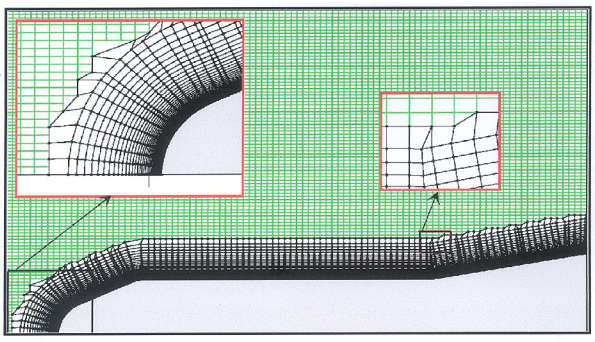

Fig.7 Hybrid Prism Layer Stitched with Outer Cartesian Mesh

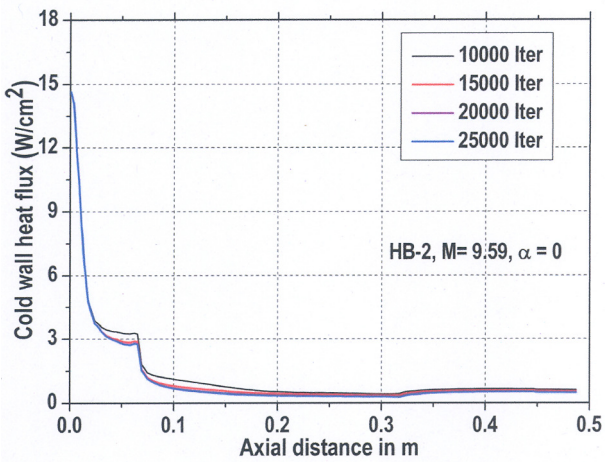

Fig.8 Iteration Convergence for Hybrid Solution for 20 mm Prism Layer

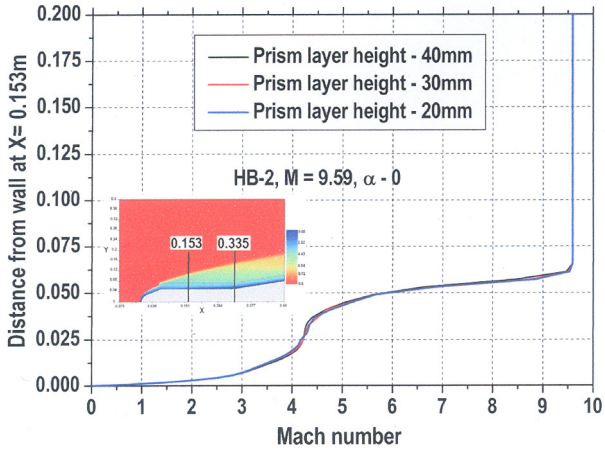

Fig.9 Mach Number Profile at X = 0.153m

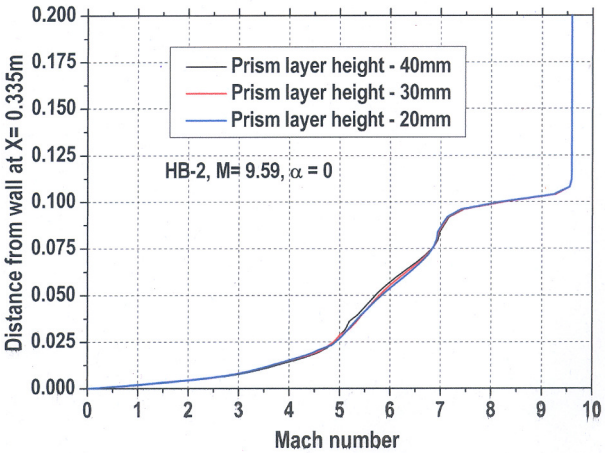

Fig.10 Mach Number Profile at X = 0.335 m

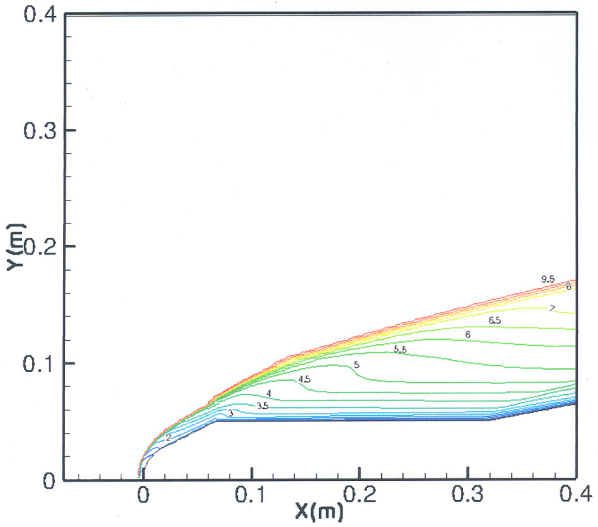

Fig.11 Mach Line Contours Over the Geometry

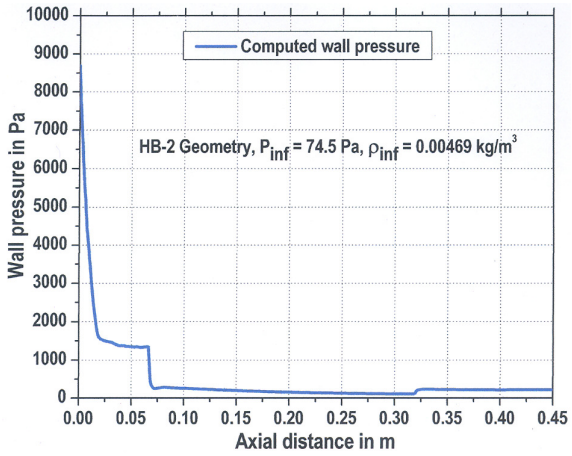

Fig.12 Boundary Layer Edge Static Pressure Along the Body Obtained from Inviscid Solution

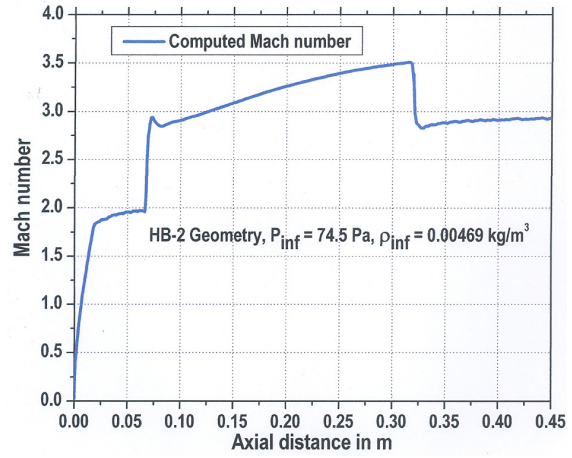

Fig.13 Boundary Layer Edge Mach Number Along the Body Obtained from Inviscid Solution

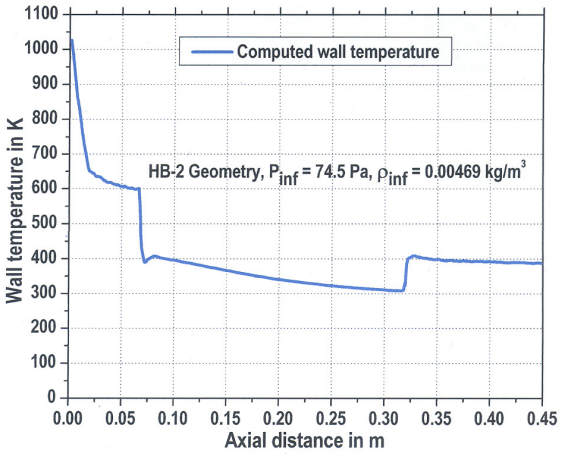

Fig.14 Boundary Layer Edge Static Temperature from Inviscid Solution

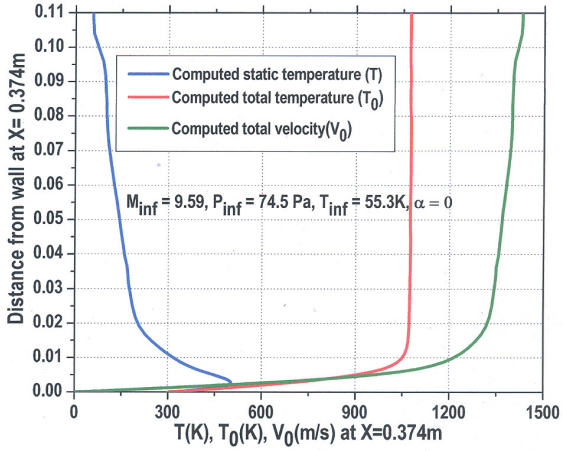

Fig.15 Profiles of Total Velocity and Static and Total Temperture at X = 0.374 m

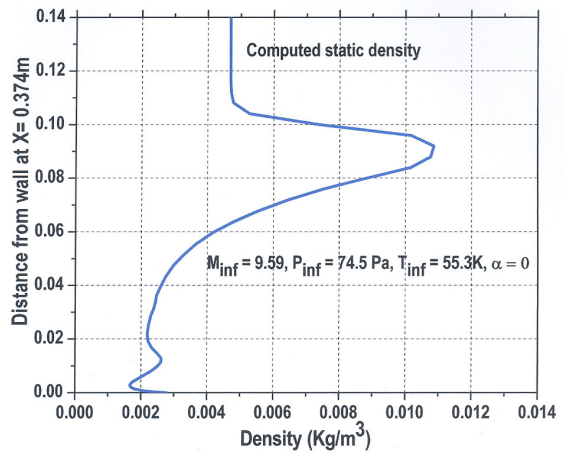

Fig.16 Profile of Static Density at Location 0.374 m from Nose

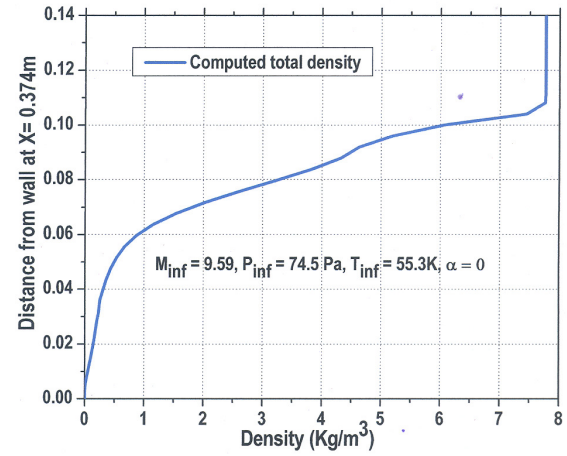

Fig.17 Stagnation Density Profile at Location 0.374 m from Nose

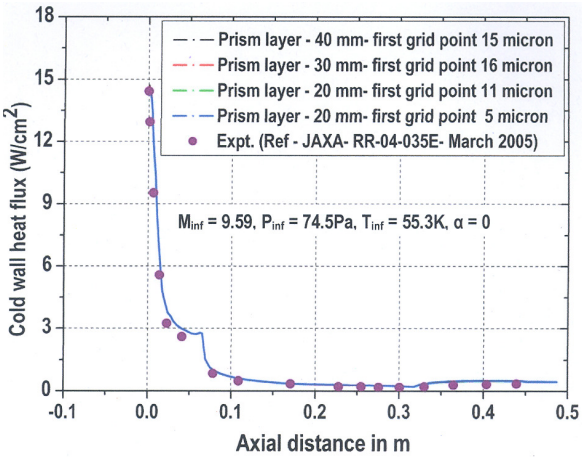

Fig.18 Comparison of Heat Flux along the Wall for Different Prism Layer Grids

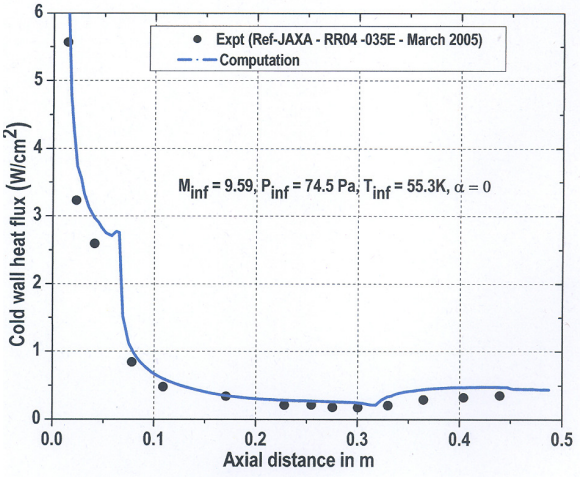

Fig.19 Enlarged View of Heat Flux along the Wall

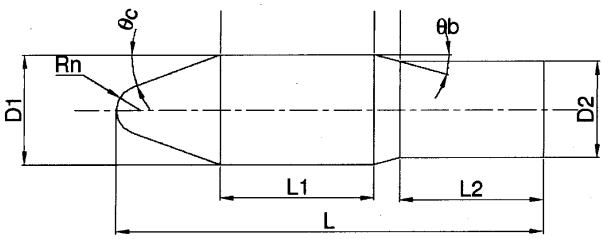

Fig.20 Schematic of a Typical Bulbous Heat Shield

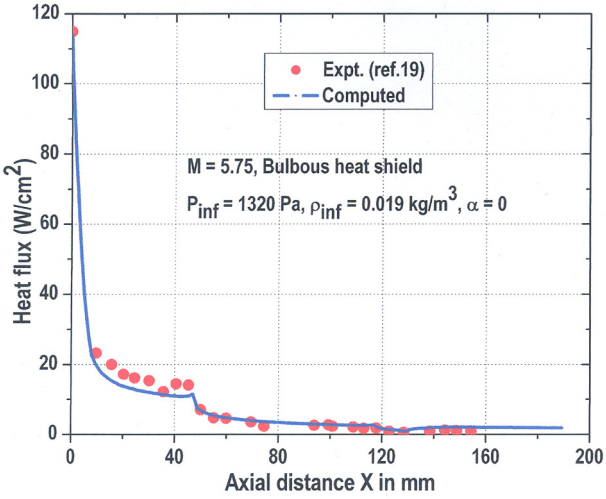

Fig.21 Cold Wall Heat Flux along the Wall of the Bulbous Heat Shield

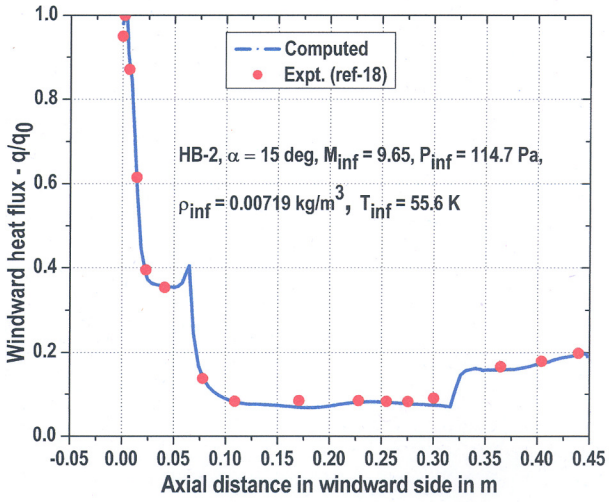

Fig.22 Cold Wall Heat Flux Distribution along the Windward Side of HB-2 Geometry at Angle of Attack 15°